
Directional Sign Loss: A Topology-Preserving Loss Function that Approximates the Sign of Finite Differences

Harvey Dam
harvey.dam@utah.edu

Tripti Agarwal
tripti.agarwal@utah.edu

Ganesh Gopalakrishnan
ganesh.cs.utah.edu

Kahlert School of Computing
University of Utah

Abstract

Preserving critical topological features in learned latent spaces is a fundamental challenge in representation learning, particularly for topology-sensitive data. This paper introduces directional sign loss (DSL), a novel loss function that approximates the number of mismatches in the signs of finite differences between corresponding elements of two arrays. By penalizing discrepancies in critical points between input and reconstructed data, DSL encourages autoencoders and other learnable compressors to retain the topological features of the original data. We present the mathematical formulation, complexity analysis, and practical implementation of DSL, comparing its behavior to its non-differentiable counterpart and to other topological measures. Experiments on one-, two-, and three-dimensional data show that combining DSL with traditional loss functions preserves topological features more effectively than traditional losses alone. Moreover, DSL serves as a differentiable, efficient proxy for common topology-based metrics, enabling its use in gradient-based optimization frameworks. Code for all experiments is available [here](#).

1 Introduction

Learned representations are central to modern machine learning, serving as compressed yet useful descriptions of data. While representations are often optimized for specific tasks, reconstructions are equally important, not only for downstream machine learning tasks, but also for human interpretability and applications. Standard loss functions consider only point-wise similarity, but often fail to capture topological structures in data. This can lead to reconstructions that appear to be faithful but miss geometric or structural features. While topology-aware learning methods, such as persistent homology, offer approaches to capturing these features, they are typically computationally inefficient and not differentiable, preventing their incorporation into gradient-based learning frameworks with large datasets.

Topological features capture the innate structure of data. These features include connected components, loops, and critical points (maxima, minima, and saddle points) Carlsson [2009] and are often obtained using topological data analysis (TDA) tools such as persistence diagrams. These features can be used for analyzing and visualizing the data structure, specifically for data where topology plays a vital role. Distance measures such as the Wasserstein distance describe the dissimilarity between the topological features of two pieces of data Edelsbrunner and Harer [2010]. These measures help researchers draw out relevant information while filtering out noise or irrelevant variations in the data and are useful in machine learning (ML) tasks such as classifying or clustering topology-rich data

Maljovec et al. [2013], Yan et al. [2021]. Scientific simulations, including those in fluid dynamics, physics, and weather prediction, leverage topological features to identify phenomena such as vortices, changes in atomic formation, and pressure extrema Agarwal et al. [2021], Ramamurthi et al. [2022]. Similarly, medical imaging often relies on capturing and comparing topological structures, such as gene interactions and tumors Singh et al. [2023]. Economists also examine financial networks through persistent features to detect market anomalies and gain insights into overall market behavior Mojdehi et al. [2025], Eberle and Holder [2007].

Lossy data compressors can reduce storage and data transfer requirements for ML models trained on large datasets, aiding data preprocessing, training, and inference. Compressed data also lowers memory bandwidth usage, speeding GPU or TPU operations and accelerating experiments. However, these compressors, including learnable variants, typically minimize point-wise error rather than preserve topological properties Soler et al. [2018a]. As a result, they can distort critical points or introduce new ones Diffenderfer et al. [2019], propagating errors through the data processing pipeline and leading to inaccurate outputs.

To address the interests and motivations of both topological data analysis and lossy data compression, we introduce a novel loss function that approximates the number of mismatches in the signs of finite differences between the corresponding elements of input and reconstructed data.

The key contributions in the paper are as follows:

- Directional sign loss (DSL), a differentiable measure of the dissimilarity between the critical points of two arrays.
- An analysis of its time and memory complexity, as well as a demonstration of its behavior on a simple example.
- Evaluations of learnable compressors, consisting of two simple autoencoders and one variational autoencoder, using this loss function, trained on 1-dimensional stock prices, 2-dimensional images, and 3-dimensional physics simulation states.
- Theoretical and empirical evidence that this loss function can be used as a proxy for other established measures of topological dissimilarity.

In the rest of this paper, we introduce the background and related work (§ 2.2), describe the loss function and demonstrate its behavior on a simple example (§ 3), evaluate it by training several autoencoders and discussing the results (§ 4), and suggest future work and offer our conclusion (§ 5).

2 Background and Related Work

We describe the background on autoencoders and topological data analysis, and discuss related work.

2.1 Background

2.1.1 Autoencoders

Autoencoders (AEs) Hinton and Salakhutdinov [2006] are neural networks that learn efficient representations of data by training on a reconstruction task. They consist of an encoder which transforms inputs to a lower-dimensional compressed representation, and a decoder which reconstructs the original input from the compressed representation. By optimizing them using a loss function that penalizes deviation from the original, AEs learn to capture essential features while discarding irrelevant information with respect to the loss function. Variants of AEs such as variational autoencoders (VAEs) Kingma and Welling [2022], adversarial autoencoders Makhzani et al. [2016], denoising autoencoders Vincent et al. [2008], and sparse autoencoders Schölkopf et al. [2007] introduce additional features such as generative modeling, robustness, and interpretability.

2.1.2 Topological data analysis

Critical points: A critical point of a continuous function f is a point in the domain where $\nabla f = 0$ Edelsbrunner and Harer [2010]. However, in discrete settings such as sampled fields on a grid, the definition of critical points from continuous functions does not directly apply. For vector fields, identifying critical points can require detecting sign changes in the determinants of vectors within

simplices formed from the vector field. This process involves evaluating whether replacing a vertex with zero leads to a determinant sign change, indicating a potential critical point Xia et al. [2024]. Because we focus on scalar fields (“tensors”), it is sufficient to approximate critical points by identifying locations where finite differences in some direction cross zero. If a critical point exists in an underlying continuous function f , then a zero crossing in the finite difference $\hat{f}(x+h) - \hat{f}(x)$ of the discrete approximation \hat{f} , using step size h , serves as an indicator of an approximate critical point with $O(h)$ error Powell [1981].

Persistence diagrams: A persistence diagram is a topological summary that captures the *birth* and *death* of homological features in a filtered space. Given a filtration, a nested sequence of spaces defined by a function, topological features such as connected components, loops, and voids appear and disappear at specific function values. Each feature is represented as a tuple in the persistence diagram, where the first coordinate corresponds to the function value at which the feature first appears (birth) and the second coordinate corresponds to where it disappears (death). These pairs are created using the Elder Rule, which states that when two features merge, the older one persists while the newer one disappears. Since changes in topology occur at critical points of the filtration function, persistence diagrams implicitly encode information about critical points. Persistence diagrams provide a compact representation of topological structure. For a worked-through example, see Appendix 5.1.1.

Distance measures: Several metrics quantify the dissimilarity between persistence diagrams, which in turn reflect differences in topological structure. Our work uses these metrics to evaluate the preservation of topological features between original and reconstructed data. The Wasserstein distance Malinovskii [1975] describes the cost of transforming one probability distribution into another, typically using norm order $p = 1$ or $p = 2$. The bottleneck distance is a special case of Wasserstein distance where $p = \infty$, capturing the largest discrepancy between the most dissimilar birth-death pairs. For persistence diagrams, these metrics compare differences between corresponding birth-death pairs in the two diagrams, implicitly reflecting variations in the underlying critical points of the filtration function. For a detailed description, see Appendix 5.1.3.

2.2 Related work

Lossy data compressors such as Di and Cappello [2016], Lindstrom [2014], Lakshminarasimhan et al. [2013], Lindstrom and Isenburg [2006] are usually developed to achieve a high compression ratio with an admissible fidelity loss. Other lossy compressors can perform certain operations in the compressed space Agarwal et al. [2024a,b], some of which are differentiable Agarwal et al. [2023]. Some lossy compressors aim to guarantee the preservation of a controllable set of topological features during compression Soler et al. [2018b], Yan et al. [2024], Xia et al. [2024]. These compressors mainly focus on maintaining point-wise error along with high compression speed and ratio. While some explicitly target topological feature preservation, all of these compressors are “frozen” and are not designed to adapt to specific data distributions as learnable compressors are.

Autoencoders (AEs) have been widely used as learnable compression models. Traditional AEs and their common variants focus primarily on reconstructing the input while implicitly learning a latent space using a standard reconstruction loss, without explicitly considering the structural properties of the data.

To address this limitation, several studies have explored adding topological constraints into neural network training. Topological autoencoders Moor et al. [2021] aim to preserve topological features of the input space in the latent representation. Persistence-weighted kernels Kusano et al. [2016] and persistence landscapes Bubenik [2015] have been used to regularize learned representations and improve their structural retention.

Topological layers have been used to integrate persistent homology into learning objectives Brüel-Gabrielsson et al. [2020] using level set and edge-based filters.

Topology-aware representational similarity analysis (tRSA) has appeared to characterize the topology of learned representations Lin and Kriegeskorte [2024]. Such analysis techniques can be robust to noise and individual variability, suggesting potential benefits of preserving topology.

Our approach differs from existing methods in that it does not impose constraints on the latent space or require modifications to the architecture of the AE. Instead, our loss function directly encourages the preservation of topological features across compression and decompression. By avoiding explicit

regularization of the latent representation, our method allows the AE to learn an efficient encoding while optimizing for structural fidelity in the reconstruction. This flexibility makes our approach applicable where efficiency and integrity must be balanced.

3 Directional Sign Loss

In many ML applications, one may prefer to capture directional trends and critical points. Standard loss functions such as the mean squared error (MSE) and mean absolute error (MAE) capture magnitude-based discrepancies but do not account for mismatches in directional changes across data points, e.g. finite differences. This limits their suitability in tasks where directional trends are emphasized, particularly where trends matter more than raw values.

To address this limitation, we introduce directional sign loss (DSL), a loss function that penalizes mismatches in the signs of finite differences between adjacent elements of predictions and targets. This encourages a model to align its predictions with the directional trends of the data.

3.1 Algorithm

In our notation, operations are performed on whole arrays, broadcasting where necessary, unless indexed into particular slices or elements, as is conventional in common deep learning frameworks.

One way to capture the differences in critical points between two arrays of numbers (“tensors”) is to take their finite differences in all directions. If tensor $X \in \mathbb{R}^n$ were 1-dimensional, this would amount to computing $X_{2:n} - X_{1:n-1}$, and doing the same to the other tensor, say Y . The signs of these finite differences can be expressed as integers using $\text{sign}(x) = \{1 \text{ if } x > 0, 0 \text{ if } x = 0, -1 \text{ if } x < 0\}$. Then, the number of mismatches between the signs of their finite differences would be aggregated. This serves as a measure of the dissimilarity of their critical points as defined above, whether they be minima, maxima, or saddle points. In contrast to other metrics, this focuses only on the presence and location of the critical points and not on the values that construct them. However, counting mismatches directly would not be differentiable. Thus, we use a smooth function \tanh , with a sharpness parameter s , to approximate the sign function. Our experiments include comparisons between the approximate and exact metrics.

DSL computes the total mismatch in directional trends between tensors X and $Y \in \mathbb{R}^{n_1 \times n_2 \times \dots \times n_d}$, which must have the same shape. One could be a reconstruction or approximation of the other.

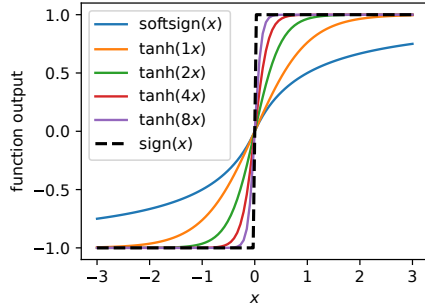


Figure 1: $\tanh(sx)$ using different values of s and other sign-like functions.

For each dimension i of the tensors from 1 to d , the following steps are performed.

1. **Compute finite differences:** Adjacent elements in each dimension are subtracted. This is done for the i th dimension for both X and Y .
2. **Approximate directional signs:** The finite differences are scaled by a sharpness factor s , and the tanh function is applied, with larger values of s producing a closer approximation to the sign function. Larger s helps distinguish DSL from other loss functions such as MAE loss, but risks vanishing gradients, making the choice of s a hyperparameter. Figure 1 shows $\tanh(sx)$ with different values of s . The user may use other sign-like functions in DSL, such as softsign Glorot and Bengio [2010].
3. **Compute mismatches:** The absolute differences between the approximated signs of the finite differences are calculated and optionally divided by two. This division matches the loss function’s units to those of a non-differentiable exact version that uses the sign function and counts mismatches directly.

The per-dimension mismatches are optionally weighted using weights $W \in \mathbb{R}^d$, allowing the user to select or emphasize certain dimensions. This also enables DSL to be applied to tensor fields by setting the elements $W_{(d-m):d}$ to zero, where m is the dimensionality of an element in the field. These weighted mismatches are then accumulated into a scalar loss value. Pseudocode is shown in Algorithm 1. In the pseudocode, $a : b$ denotes all indices from a to b . $(:)$ denotes all indices in some dimension, and $(:) * a$ denotes all indices for a sequence of a dimensions.

Algorithm 1: Directional Sign Loss (DSL)

Input: Tensors X and Y of shape (n_1, n_2, \dots, n_d) , sharpness s

Output: Loss value ℓ

$\ell \leftarrow 0$;

for $i \leftarrow 1$ **to** d **do**

Compute finite differences::

$$D_X \leftarrow X_{(:,*)^{(i-1)}, 2:n_i, (:)^{*(d-i)}} - X_{(:,*)^{(i-1)}, 1:(n_i-1), (:)^{*(d-i)}}$$

$$D_Y \leftarrow Y_{(:,*)^{(i-1)}, 2:n_i, (:)^{*(d-i)}} - Y_{(:,*)^{(i-1)}, 1:(n_i-1), (:)^{*(d-i)}}$$

Find approximate sign mismatches::

$$\Delta \leftarrow \frac{|\tanh(sD_X) - \tanh(sD_Y)|}{2}$$

With optional weights W , accumulate mismatches::

$$\ell \leftarrow \ell + (W_i \text{ or } 1) \sum \Delta$$

return ℓ

3.2 Time and memory complexity

We consider the time complexity using an idealized parallel computing model, with the availability of infinite parallel processors. If X and Y are d -dimensional arrays shaped (n_1, n_2, \dots, n_d) , we could create all Δ arrays for each dimension in constant time. Then, all Δ , containing a total of $d \prod_{i=1}^d (n_i - 1)$ elements, are summed. Ignoring the subtraction of 1 for large n_i , this takes $O(\log_2(d \prod_{i=1}^d n_i))$ time. Taking the logarithm of the product, we have $O(\log_2 d + \sum_{i=1}^d \log_2 n_i)$.

However this would take $O(d \prod_{i=1}^d n_i)$ memory. Our implementation resembles the pseudocode in Algorithm 1, where the mismatches are summed separately per dimension. This has a complexity of

$$O\left(d \sum_{i=1}^d \log_2 n_i\right) \text{ time, } O\left(\prod_{i=1}^d n_i\right) \text{ memory.}$$

For comparison, MSE has a time complexity of $O(\sum_{i=1}^d \log_2 n_i)$ and the same memory complexity. Making persistence diagrams and taking the Wasserstein distance between them takes $O(\prod_{i=1}^d n_i^3)$ time and $O(\prod_{i=1}^d n_i)$ memory.

Implementation notes:

- In our implementation, we skip the main calculation for the first (batch) dimension and provide options for reduction (mean, sum, or none), resembling typical PyTorch loss functions.
- If the option to match the units of the exact version of DSL (using sign instead of tanh) is turned off, we scale the return value by the number of comparisons, making it easier to use in combination with conventional loss functions such as MSE loss.
- As the choice of s greatly affects the behavior of the loss function, we provide an approach to learn s in Appendix 5.3.

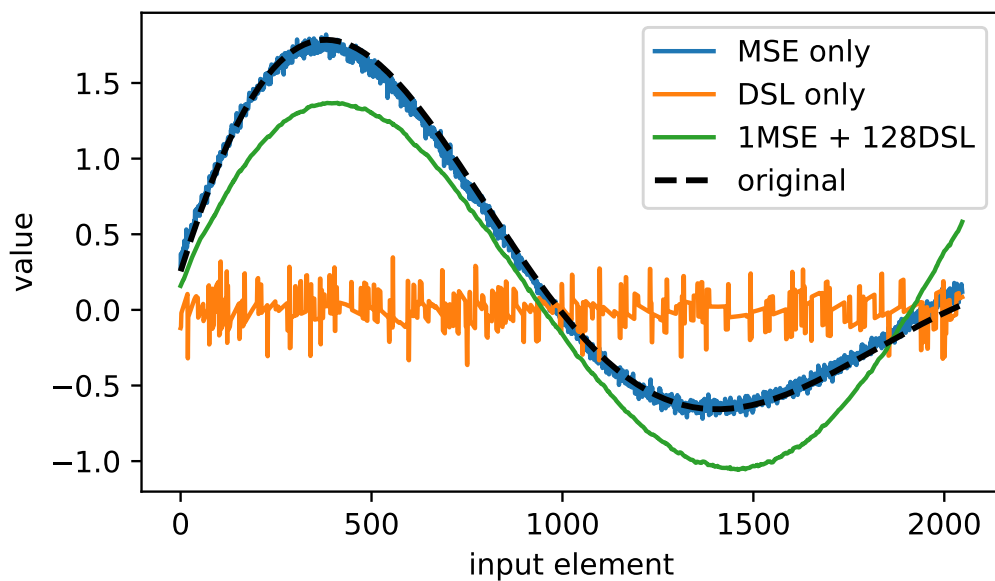
3.3 Demonstration

To illustrate DSL’s behavior, we use a simple example. We trained a simple autoencoder consisting of 2-layer perceptrons with ReLU between the layers for both the encoder and the decoder on a generated dataset. The dataset consists of 2048 points on one cycle of a sinusoidal wave, starting at some random point in the cycle, i.e. $\sin([0 : 2\pi] + U(0, 2\pi))$, scaled by $e^{[-1:1]}$ with 0.5 probability and $e^{[1:-1]}$ with 0.5 probability. The autoencoder compressed the data to a latent dimensionality of 2.

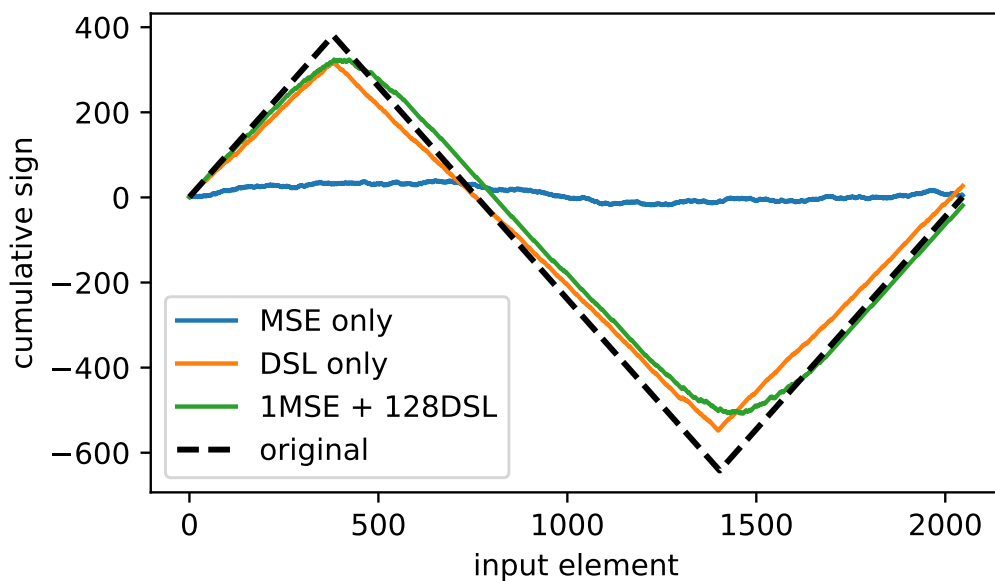
Figure 2a shows an example and its reconstruction after training with the conventional MSE loss, DSL only with $s = 32$, and a combination of 1 MSE + 128 DSL. This may appear imbalanced, but was necessary for DSL to have an obvious effect on training, as the MSE loss value was usually about 150 times the DSL value (Table 1). As expected, using MSE loss gives the closest reconstruction, but exhibits many direction changes compared to the original. Using only DSL, one may expect it to ideally go up or down linearly until the crest or trough of the wave, but this is not what happens. The reconstruction stays close to 0 while following the direction of the original curve, occasionally jumping back. This tendency arises from a combination of the low latent dimensionality and the properties of DSL. Outputs are encouraged to stay near 0 to avoid large penalties from mismatches and to allow the parameters to easily change the direction of the trend, as all it has to do is get the direction right. While the jump across 0 may appear large from the perspective of the absolute value of finite differences, they only cost one wrong sign in DSL.

Figure 2b shows the cumulative signs, which increase by 1 when the sign of the finite difference is positive, and decrease if it is negative. This can be thought of as the ideal output using only DSL. We expect constantly increasing or decreasing cumulative signs, which change directions at a sharp point, i.e. a sawtooth wave which is reflected in the original. Using the combination of the loss functions, the reconstruction exhibits characteristics of both previous cases, showing a curve that resembles the shape of the original curve, with mostly the same trends, and a more sawtooth-like cumulative signs curve.

Table 1 shows several metrics after training with different loss functions. In the table, “Exact DSL” refers to the non-differentiable error metric mentioned in § 3.1 that uses the sign function. As expected, the model trained with only DSL performed best on this metric. “Persistence” refers to the Wasserstein distance between persistence diagrams of the inputs and reconstructions, a common way to compare topological features. We only created 0-dimensional persistence diagrams (not to be confused with tensor dimensionality), as higher-dimensional diagrams were impractically expensive (Appendix 5.1.1). The model trained on only DSL, although encouraged to preserve trends, did not perform best in persistence diagram distance because persistence diagrams account for codomain values of critical points, and are thus sensitive to raw values. The model trained on the 1 MSE + 128



(a) Original vs reconstructions values.



(b) Original vs reconstructions cumulative signs.

Figure 2: Example originals and reconstructions of the generated sinusoidal wave dataset. The cumulative signs (2b) increase by 1 when the sign of the finite difference is positive, and decreases if it is negative. The combination of training with 1 MSE + 128 DSL results in reconstructions that have similar shape to the original and have movement directions like those of the original.

| Training Loss Function | Evaluation Metrics After Training | | | |
|------------------------|-----------------------------------|---------------|-----------------|---------------|
| | MSE | DSL | Exact DSL | Persistence |
| MSE | 23.3221 | 0.5920 | 968.1504 | 0.6992 |
| DSL | 1887.9517 | 0.1471 | 194.4619 | 2.0775 |
| 1 MSE + 128 DSL | 185.3973 | 0.0944 | 429.5840 | 0.4317 |

Table 1: Loss-like metrics after training the 2-layer perceptron autoencoder on the sinusoidal dataset with different loss functions. The first column lists the loss function used for training, while the remaining columns contain evaluation metrics after training. ‘‘Persistence’’ denotes the Wasserstein distance between persistence diagrams of the inputs and reconstructions. The reconstructions from the model trained with 1 MSE + 128 DSL had the closest persistence diagrams to those of the originals.

| Training Loss Function | Evaluation Metrics After Training | | | |
|------------------------|-----------------------------------|---------------|----------------|---------------|
| | MSE | DSL | Exact DSL | Persistence |
| MSE | 3.3800 | 0.5847 | 21.4571 | 0.7007 |
| DSL | 177.4241 | 0.5410 | 20.0137 | 2.3836 |
| 1 MSE + 100 DSL | 4.3236 | 0.5677 | 20.9642 | 0.8034 |

Table 2: Loss-like metrics after training the 2-layer perceptron autoencoder on NVDA stock prices. Adding DSL to the loss function leads to better performance on the exact DSL metric, but results in greater persistence diagram distance, in which the slightly higher proportion of correct directions exhibited by the DSL and mixture models was not enough to compensate for the deviation from the raw prices.

DSL mixture performed best on this metric because it balanced preserving values and preserving trends.

This demonstration shows two extremes in a continuum of loss function choice. From the perspective of conventional distances, MSE does well and DSL does poorly, while from the perspective of behavior comparison, DSL does well while MSE does poorly. Note that we used a low latent dimensionality of 2 to emphasize the differences between loss functions. If it were increased to 4, all reconstructions except that using DSL only would closely overlap and follow the original. This suggests that in the typical case, where the preservation of trends is relevant, a mixture of loss functions would give the most desirable result.

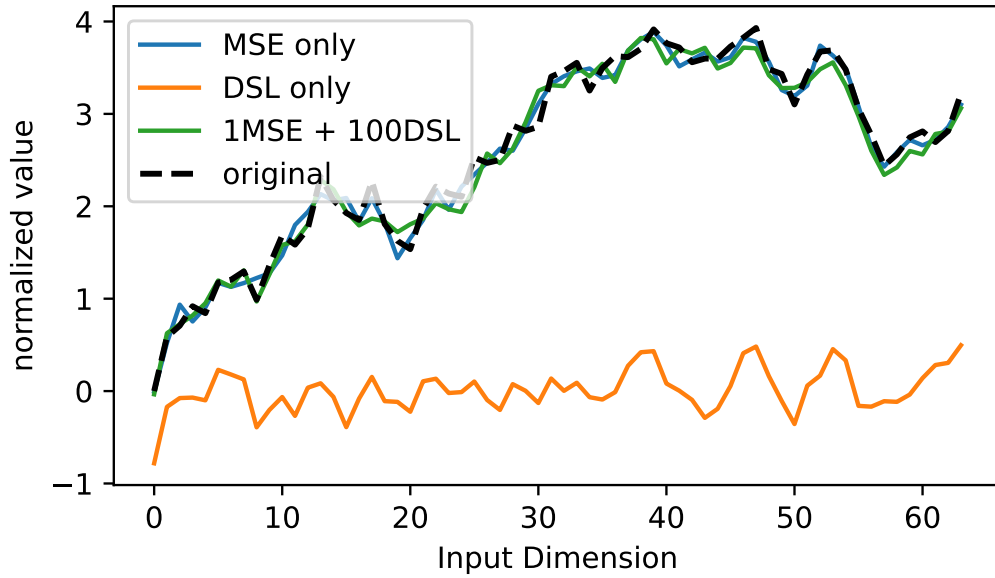
4 Experiments

DSL can be used with MSE loss in most learnable compressor training processes. To assess its impact, we trained autoencoders on 1-dimensional stock prices, 2-dimensional images, and 3-dimensional physics simulation states. Hyperparameters are in Table 4. For details, see the code.

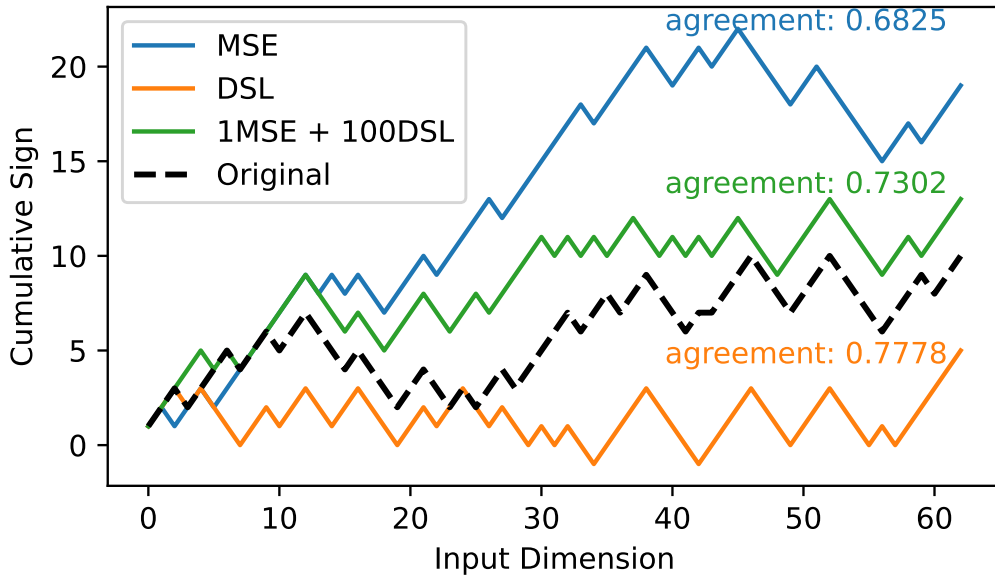
4.1 Stock prices

Stock prices are challenging to compress because price changes resemble Brownian motion Samuelson [2015]. Certain trading strategies focus on the direction of price changes instead of the magnitude or absolute price Bakhach et al. [2016], Aloud [2015]. We downloaded minute-level prices of NVDA from 2024-12-24 to 2025-01-22, totaling 15360 prices. We sampled subsequences of 64 minutes, normalized them to start at 0, and divided them by the overall standard deviation. The autoencoder had a 2-layer perceptron encoder and decoder with ReLU between layers. The latent dimensionality was 32.

Figure 3 shows an example reconstruction after training with MSE loss only, DSL only with $s = 16$, and a combination of 1 MSE + 100 DSL. As expected, the reconstruction using only DSL stayed near 0, but the other reconstructions followed the original price closely. The differences between them are more obvious in Figure 3b, which illustrates that the DSL reconstruction more frequently moved in the same direction as the original compared to the others. The combination loss reconstruction



(a) Original normalized prices vs reconstructions values.



(b) Original vs reconstructions cumulative signs.

Figure 3: Original normalized stock prices vs reconstructions after training a simple autoencoder using MSE, DSL, or a combination of 1 MSE + 100 DSL. In 3b, “agreement” is the proportion of finite difference signs that are the same as those of the original. While in 3a, the MSE and combination curves both follow the original closely, in 3b, the DSL curve moves in the same direction most often, with the combination in second place.

| Training Loss Function | Evaluation Metrics After Training | | | | | |
|------------------------|-----------------------------------|---------------|---------------|--------------------|---------------|----------------|
| | BPP | MSE | DSL | Exact DSL | Persistence | PSNR |
| MSE | 0.3553 | 0.0012 | 0.9953 | 1197730.9583 | 0.1933 | 29.5401 |
| DSL | 2.4361 | 0.0369 | 0.9741 | 1124641.7917 | 0.4650 | 14.9261 |
| 0.5 MSE + 0.5 DSL | 7.2529 | 0.0001 | 0.1854 | 456662.6250 | 0.1088 | 41.5673 |

Table 3: Evaluation metrics after training the model with different loss functions. Bits per pixel (BPP) quantifies the compression and quality trade-off in a VAE, and peak signal-to-noise ratio (PSNR) is a measurement of the distortion or noise in a signal compared to a reference, where higher is better. With the combination 0.5 MSE + 0.5 DSL, the model achieves the best performance on all metrics except BPP.

showed a lower agreement rate than the DSL reconstruction but was still higher than when using MSE loss alone.

Table 2 shows loss-like metrics after training. As we expect, the models trained using MSE and DSL perform best on the MSE and (exact) DSL metrics respectively. What may be unexpected is that persistence diagram distance was best when using MSE alone. This can be explained by considering the data: the Brownian-like motion of stock prices appears as unstructured noise on the relatively short-term scale of minutes, leading to a high proportion of incorrect directions in all reconstructions. The MSE reconstructions, and to some extent the 1 MSE + 100 DSL reconstructions, made up for it by having reconstructions with closer values to the original.

4.2 Images

The field of learnable data compressors has had the most study in the domain of image compression, particularly using variational autoencoders (VAEs), which are autoencoders whose latent representations are encouraged to be normally distributed. This allows generating new images by sampling from the normal latent distribution. We trained a quantization-aware ResNet-based VAE designed for image compression Duan et al. [2024], using MSE loss, DSL, and 0.5 MSE + 0.5 DSL. We used Algorithm 2 on COCO 2017 Lin et al. [2014], the training dataset, to find a sharpness of 9.6.

Table 3 shows loss-like metrics after training using MSE, DSL, or 0.5 MSE + 0.5 DSL. The table introduces the image-oriented metrics bits per pixel (BPP) and peak signal-to-noise ratio (PSNR). BPP is the average number of bits needed to encode each pixel, computed from the negative log-likelihood of the image under the model and the Kullback–Leibler (KL) divergence between the approximate posterior and the prior. PSNR is the scaled logarithm of the squared dynamic range divided by the MSE, a measurement of the distortion or noise in a signal compared to a reference, often used in image and audio processing. The model trained using 0.5 MSE + 0.5 DSL achieved the best scores on all metrics except BPP. This is likely due to the training scheme which attempts to balance BPP and loss by randomly choosing a reconstruction loss factor per training iteration, relative to a constant KL divergence loss factor Duan et al. [2024].

Figure 4 shows an example image from the Kodak Lossless True Color Image Suite Eastman Kodak Company [1999] and its reconstructions, using the lowest reconstruction loss weight of 16, encouraging minimum bit rate. The only visible differences among the reconstructions are that using only DSL, the reconstruction tends to stay close to the middle of the dynamic range, resulting in a faded-looking reconstruction. This reflects the tendency of the reconstruction to stay near zero in § 3.3.

4.3 Physical simulations

Shallow water simulations model fluid flow under the assumption that the water surface dimensions are much larger than its depth, which allows the simulations to avoid modeling vertical fluid velocity. These simulations solve a set of partial differential equations that describe the conservation of mass and momentum in a fluid layer, and can output surface height and fluid velocities on horizontal axes. We used a simulation to generate data for evaluating DSL on a 3-dimensional dataset. Alternative datasets such as SDRBench Zhao et al. [2020] had only hundreds of examples or were best described as 2-dimensional with multiple channels (e.g. images). Our simulation initializes a shallow container



Figure 4: An example image and its reconstructions from the validation dataset Eastman Kodak Company [1999]. Using only DSL (4c), the reconstruction tends to stay close to the middle of the dynamic range, resulting in a faded-looking reconstruction. We cannot see any differences between the others and the original.

of water with a Gaussian bump-shaped high spot in a random location. As time steps progress, the bump falls and the water moves around. We take snapshots of the water surface height and return batches of examples shaped (number of snapshots, container length, container width). For this experiment, examples are shaped (8, 64, 64). On this dataset, we trained an autoencoder with two 3-dimensional convolutional layers for both the encoder and decoder, with ReLU between layers. DSL sharpness was 16.

Figure 5 shows loss-like metrics after training on mixtures of MSE and DSL at varying proportions. Persistence diagram distance appears to peak at 0.7 MSE + 0.3 DSL. This can be interpreted as not achieving reconstruction fidelity in terms of raw values while also not faithfully reproducing the directional trends. At other points in the domain, we observe expected training behavior, where MSE loss is minimized when MSE weight is highest, and DSL loss and similar metrics are minimized where DSL weight is highest.

The minimum persistence diagram distance is achieved when using only DSL, but this results in the jumping-across-zero patterns that we observed in § 3.3, as visible in Figure 6c. These patterns, which repeat every 4 elements, correspond to the mapping between the convolutional decoders and their inputs, where each input element corresponds to a $4 \times 4 \times 4$ block in the reconstruction. This suggests that the convolutional decoder layers have learned to output the correct water surface height gradients while the other layers may have focused on other features.

5 Conclusion and Future work

We introduced a novel loss function, directional sign loss (DSL) and investigated its properties and effects on training a variety of autoencoders on diverse datasets. We found that DSL, when used in combination with MSE loss, can serve as a proxy for common non-differentiable and computationally

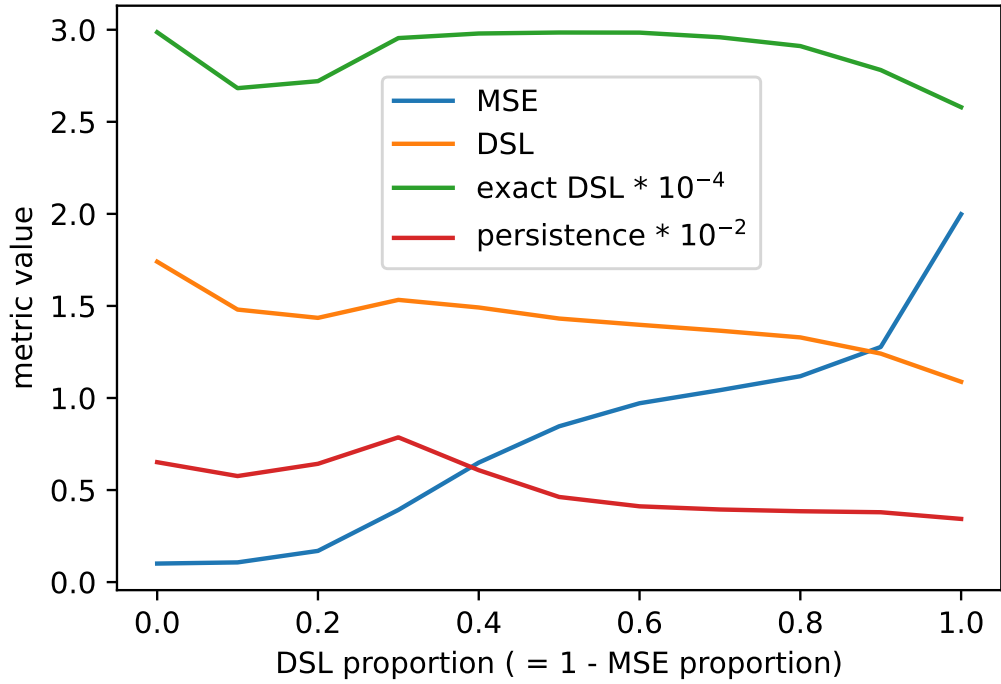


Figure 5: Loss-like metrics after training the 3-dimensional autoencoder on shallow water simulations using a mixture of MSE and DSL, with ranging from 1.0 MSE + 0.0 DSL to 0.0 MSE + 1.0 DSL in steps of 0.1. Because the metrics use different units, some are scaled so that their trends are easily comparable. Persistence diagram distance is minimized when using only DSL, but MSE is worst using that scheme. 0.9 MSE + 0.1 DSL (near the left side) appears to balance all metrics while occupying the local minimum in exact DSL.

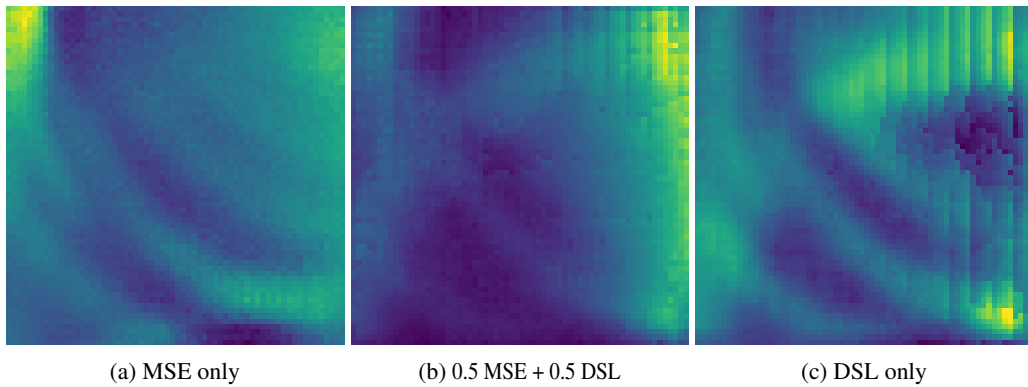


Figure 6: Reconstructions using some mixtures of MSE and DSL. For the full figure, see Appendix 7. Block-shaped patterns appear in the reconstructions using a high proportion of DSL, corresponding to the upsampling factor of 2 in the two convolutional decoders.

expensive topological feature descriptors, namely the Wasserstein distance between persistence diagrams, and can encourage autoencoders to preserve topological features such as critical points in their reconstructions while maintaining or minimally sacrificing performance on traditional metrics.

For future work, because we have observed that learning behavior is sensitive to the balance of DSL and traditional loss functions, we anticipate a way to find an optimal balance, facilitating hyperparameter search. Also, although adjusting the per-dimensional weights of DSL can enable its use for vector fields and higher-dimensional fields, we have not explored this aspect. Finally, while DSL can be introduced into the training process of any typical autoencoder, we have not yet explored model architectures besides MLPs and CNNs. A task requiring a transformer-based autoencoder would bring additional insights into DSL's effects.

Acknowledgments and Disclosure of Funding

Supported in part by NSF CISE Award 2217154.

References

- Gunnar Carlsson. Topology and data. *Bulletin of the American Mathematical Society*, 46(2):255–308, 2009.
- Herbert Edelsbrunner and John Harer. *Computational Topology: An Introduction*. American Mathematical Soc., 2010.
- Dan Maljovec, Bei Wang, Valerio Pascucci, Peer-Timo Bremer, and Diego Mandelli. Analyzing dynamic probabilistic risk assessment data through topology-based clustering. In *Proceedings of the ANS PSA 2013 International Topical Meeting on Probabilistic Safety Assessment and Analysis*, 2013.
- Lin Yan, Talha Bin Masood, Raghavendra Sridharamurthy, Farhan Rasheed, Vijay Natarajan, Ingrid Hotz, and Bei Wang. Scalar field comparison with topological descriptors: Properties and applications for scientific visualization. *Computer Graphics Forum*, 40(3):599–633, 2021. doi: 10.1111/cgf.14331.
- Tripti Agarwal, Amit Chattopadhyay, and Vijay Natarajan. Topological feature search in time-varying multifield data. In Ingrid Hotz, Talha Bin Masood, Filip Sadlo, and Julien Tierny, editors, *Topological Methods in Data Analysis and Visualization VI*, pages 197–217, Cham, 2021. Springer International Publishing. ISBN 978-3-030-83500-2.
- Yashwanth Ramamurthi, Tripti Agarwal, and Amit Chattopadhyay. A topological similarity measure between multi-resolution reeb spaces. *IEEE Transactions on Visualization and Computer Graphics*, 28(12):4360–4374, 2022. doi: 10.1109/TVCG.2021.3087273.
- Yashbir Singh, Colleen M Farrelly, Quincy A Hathaway, Tim Leiner, Jaidip Jagtap, Gunnar E Carlsson, and Bradley J Erickson. Topological data analysis in medical imaging: current state of the art. *Insights into Imaging*, 14(1):58, 2023.
- Kosar Farajpour Mojdehi, Babak Amiri, and Amirali Haddadi. A novel hybrid model for credit risk assessment of supply chain finance based on topological data analysis and graph neural network. *IEEE Access*, 13:13101–13127, 2025. doi: 10.1109/ACCESS.2025.3528373.
- William Eberle and Lawrence Holder. Anomaly detection in data represented as graphs. *Intelligent Data Analysis*, 11(6):663–689, 2007.
- Maxime Soler, Melanie Plainchault, Bruno Conche, and Julien Tierny. Topologically Controlled Lossy Compression. In *2018 IEEE Pacific Visualization Symposium (PacificVis)*, pages 46–55, Los Alamitos, CA, USA, April 2018a. IEEE Computer Society. doi: 10.1109/PacificVis.2018.00015. URL <https://doi.ieeecomputersociety.org/10.1109/PacificVis.2018.00015>.
- James Diffenderfer, Alyson L. Fox, Jeffrey A. Hittinger, Geoffrey Sanders, and Peter G. Lindstrom. Error analysis of zfp compression for floating-point data. *SIAM Journal on Scientific Computing*, 41(3):A1867–A1898, January 2019. ISSN 1095-7197. doi: 10.1137/18m1168832. URL <http://dx.doi.org/10.1137/18M1168832>.

- G. E. Hinton and R. R. Salakhutdinov. Reducing the dimensionality of data with neural networks. *Science*, 313(5786):504–507, 2006. doi: 10.1126/science.1127647. URL <https://www.science.org/doi/abs/10.1126/science.1127647>.
- Diederik P Kingma and Max Welling. Auto-encoding variational bayes, 2022. URL <https://arxiv.org/abs/1312.6114>.
- Alireza Makhzani, Jonathon Shlens, Navdeep Jaitly, Ian Goodfellow, and Brendan Frey. Adversarial autoencoders, 2016. URL <https://arxiv.org/abs/1511.05644>.
- Pascal Vincent, Hugo Larochelle, Yoshua Bengio, and Pierre-Antoine Manzagol. Extracting and composing robust features with denoising autoencoders. In *Proceedings of the 25th International Conference on Machine Learning, ICML '08*, page 1096–1103, New York, NY, USA, 2008. Association for Computing Machinery. ISBN 9781605582054. doi: 10.1145/1390156.1390294. URL <https://doi.org/10.1145/1390156.1390294>.
- Bernhard Schölkopf, John Platt, and Thomas Hofmann. *Efficient Learning of Sparse Representations with an Energy-Based Model*, pages 1137–1144. 2007.
- Mingze Xia, Sheng Di, Franck Cappello, Pu Jiao, Kai Zhao, Jinyang Liu, Xuan Wu, Xin Liang, and Hanqi Guo. Preserving topological feature with sign-of-determinant predicates in lossy compression: A case study of vector field critical points. In *2024 IEEE 40th International Conference on Data Engineering (ICDE)*, pages 4979–4992, 2024. doi: 10.1109/ICDE60146.2024.00378.
- Michael J. D. Powell. *Approximation Theory and Methods*. Cambridge University Press, Cambridge, UK, 1981.
- V. A. Malinovskii. Markovskie protsessy na schetnom proizvedenii prostranstv, opisivayushchie bol'shie sistemy avtomatov. *Teoriya veroyatnostei i ee primeneniya*, 20(1):83–101, 1975.
- Sheng Di and Franck Cappello. Fast error-bounded lossy hpc data compression with sz. In *2016 IEEE International Parallel and Distributed Processing Symposium (IPDPS)*, pages 730–739, 2016. doi: 10.1109/IPDPS.2016.11.
- Peter Lindstrom. Fixed-rate compressed floating-point arrays. *IEEE Transactions on Visualization and Computer Graphics*, 20(12):2674–2683, 2014. doi: 10.1109/TVCG.2014.2346458.
- Sriram Lakshminarasimhan, Neil Shah, Stephane Ethier, Seung-Hoe Ku, C. S. Chang, Scott Klasky, Rob Latham, Rob Ross, and Nagiza F. Samatova. Isabela for effective in situ compression of scientific data. *Concurrency and Computation: Practice and Experience*, 25(4):524–540, 2013. doi: <https://doi.org/10.1002/cpe.2887>. URL <https://onlineibrary.wiley.com/doi/abs/10.1002/cpe.2887>.
- Peter Lindstrom and Martin Isenburg. Fast and efficient compression of floating-point data. *IEEE Transactions on Visualization and Computer Graphics*, 12(5):1245–1250, 2006. doi: 10.1109/TVCG.2006.143.
- Tripti Agarwal, Sheng Di, Jiajun Huang, Yafan Huang, Ganesh Gopalakrishnan, Robert Underwood, Kai Zhao, Xin Liang, Guanpeng Li, and Franck Cappello. Szops: Scalar operations for error-bounded lossy compressor for scientific data. In *SC24-W: Workshops of the International Conference for High Performance Computing, Networking, Storage and Analysis*, pages 260–269, 2024a. doi: 10.1109/SCW63240.2024.00042.
- Tripti Agarwal, Sheng Di, Jiajun Huang, Yafan Huang, Ganesh Gopalakrishnan, Robert Underwood, Kai Zhao, Xin Liang, Guanpeng Li, and Franck Cappello. Hoszp: An efficient homomorphic error-bounded lossy compressor for scientific data, 2024b. URL <https://arxiv.org/abs/2408.11971>.
- Tripti Agarwal, Harvey Dam, Ponnuswamy Sadayappan, Ganesh Gopalakrishnan, Dorra Ben Khalifa, and Matthieu Martel. What operations can be performed directly on compressed arrays, and with what error? In *Proceedings of the SC '23 Workshops of The International Conference on High Performance Computing, Network, Storage, and Analysis, SC-W '23*, page 254–262, New York, NY, USA, 2023. Association for Computing Machinery. ISBN 9798400707858. doi: 10.1145/3624062.3625122. URL <https://doi.org/10.1145/3624062.3625122>.

- Maxime Soler, Mélanie Plainchault, Bruno Conche, and Julien Tierny. Topologically controlled lossy compression. In *2018 IEEE Pacific Visualization Symposium (PacificVis)*, pages 46–55, 2018b. doi: 10.1109/PacificVis.2018.00015.
- Lin Yan, Xin Liang, Hanqi Guo, and Bei Wang. Toposz: Preserving topology in error-bounded lossy compression. *IEEE Transactions on Visualization and Computer Graphics*, 30(1):1302–1312, 2024. doi: 10.1109/TVCG.2023.3326920.
- Michael Moor, Max Horn, Bastian Rieck, and Karsten Borgwardt. Topological autoencoders, 2021. URL <https://arxiv.org/abs/1906.00722>.
- Genki Kusano, Kenji Fukumizu, and Yasuaki Hiraoka. Persistence weighted gaussian kernel for topological data analysis, 2016. URL <https://arxiv.org/abs/1601.01741>.
- Peter Bubenik. Statistical topological data analysis using persistence landscapes. *Journal of Machine Learning Research*, 16(1):77–102, 2015.
- Rickard Brüel-Gabrielsson, Bradley J. Nelson, Anjan Dwaraknath, Primoz Skraba, Leonidas J. Guibas, and Gunnar Carlsson. A topology layer for machine learning, 2020. URL <https://arxiv.org/abs/1905.12200>.
- Baihan Lin and Nikolaus Kriegeskorte. The topology and geometry of neural representations. *Proceedings of the National Academy of Sciences*, 121(42), October 2024. ISSN 1091-6490. doi: 10.1073/pnas.2317881121. URL <http://dx.doi.org/10.1073/pnas.2317881121>.
- Xavier Glorot and Yoshua Bengio. Understanding the difficulty of training deep feedforward neural networks. In *Proceedings of the 13th International Conference on Artificial Intelligence and Statistics (AISTATS)*, volume 9 of *Proceedings of Machine Learning Research*, pages 249–256. PMLR, 2010.
- Paul A. Samuelson. Proof that Properly Anticipated Prices Fluctuate Randomly. In Anastasios G Malliaris and William T Ziemba, editors, *THE WORLD SCIENTIFIC HANDBOOK OF FUTURES MARKETS*, World Scientific Book Chapters, chapter 2, pages 25–38. World Scientific Publishing Co. Pte. Ltd., August 2015.
- Amer Bakhach, Edward Tsang, Wing Lon Ng, and V L Raju Chinthalapati. Backlash agent: A trading strategy based on directional change. In *2016 IEEE Symposium Series on Computational Intelligence (SSCI)*, pages 1–9, 2016. doi: 10.1109/SSCI.2016.7850004.
- Monira Essa Aloud. Directional-change event trading strategy: Profit-maximizing learning strategy. In *Seventh International Conference on Advanced Cognitive Technologies and Applications*, 2015. URL https://personales.upv.es/thinkmind/dl/conferences/cognitive/cognitive_2015/cognitive_2015_6_20_40112.pdf.
- Zhihao Duan, Ming Lu, Jack Ma, Yuning Huang, Zhan Ma, and Fengqing Zhu. Qarv: Quantization-aware resnet vae for lossy image compression. *IEEE Transactions on Pattern Analysis and Machine Intelligence*, 46(1):436–450, January 2024. ISSN 1939-3539. doi: 10.1109/tpami.2023.3322904. URL <http://dx.doi.org/10.1109/TPAMI.2023.3322904>.
- Tsung-Yi Lin, Michael Maire, Serge Belongie, James Hays, Pietro Perona, Deva Ramanan, Piotr Dollár, and C Lawrence Zitnick. Microsoft coco: Common objects in context. *arXiv preprint arXiv:1405.0312*, 2014.
- Eastman Kodak Company. Kodak lossless true color image suite, 1999. URL <http://r0k.us/graphics/kodak/>. Accessed: 2025-01-29.
- K. Zhao, S. Di, X. Liang, S. Li, D. Tao, J. Bessac, Z. Chen, and F. Cappello. SDRBench: Scientific data reduction benchmark for lossy compressors. In *International Workshop on Big Data Reduction (IWBDR2020)*, in conjunction with *IEEE BigData20*, 2020. URL <https://sdrbench.github.io>.
- Diederik P. Kingma and Jimmy Ba. Adam: A method for stochastic optimization, 2017. URL <https://arxiv.org/abs/1412.6980>.

Kaiming He, Xiangyu Zhang, Shaoqing Ren, and Jian Sun. Delving deep into rectifiers: Surpassing human-level performance on imagenet classification, 2015. URL <https://arxiv.org/abs/1502.01852>.

Dan Hendrycks and Kevin Gimpel. Gaussian error linear units (gelus), 2023. URL <https://arxiv.org/abs/1606.08415>.

Appendix

5.1 Making 0-dimensional persistence diagrams and taking the Wasserstein distance between them

Creating 0-dimensional persistence diagrams from tensors involves analyzing the connected components of sublevel sets of the scalar field defined by the tensor.

Input: The input is a tensor T of arbitrary dimensionality d , representing a scalar field $f : X \rightarrow \mathbb{R}$, where X is a d -dimensional grid.

5.1.1 Persistence diagram

To analyze the topology of the scalar field, we consider its sublevel sets $X_t = \{x \in X \mid f(x) \leq t\}$. As the threshold t increases, the sublevel sets X_t change, and we can track how their topology evolves. This process creates a filtration, a sequence of nested subspaces $X_{t_1} \subseteq X_{t_2} \subseteq \dots \subseteq X_{t_n}$.

To build a persistence diagram,

1. Flatten the tensor into a list of scalar values and their corresponding grid positions.
2. Sort the values in ascending order: $f_1 \leq f_2 \leq \dots \leq f_m$ where m is the total number of grid points.
3. Use a union-find data structure to keep track of connected components. Initialize each grid point as its own component.
4. For each point x_i in order of increasing $f(x_i)$:
 - (a) If x_i is a local minimum (i.e., all its neighbors in the grid have higher values), a new connected component is born. The definition of *neighbors* for each grid point is its orthogonally and diagonally adjacent elements. For a d -dimensional grid, each point has $3^d - 1$ neighbors.
 - In 1D, each element has up to 2 neighbors.
 - In 2D, each pixel has up to 8 neighbors.
 - In 3D, each voxel has up to 26 neighbors.
 - (b) If x_i connects two existing components, the younger component dies and merges into the older one.
 - (c) For each component, record its birth time (when it appears) and death time (when it merges with another component). A component that never dies is recorded as having a death time of $+\infty$.

Time and memory complexity

The time complexity for computing a 0D persistence diagram for a tensor is:

- Sorting: $O(\log m)$ using parallel sorting, where m is the number of grid points.
- Union-find operations: $O(m\alpha(m))$, where $\alpha(m)$ is the inverse Ackermann function (effectively constant).

For storing simplices, $O(m^d)$ memory is necessary, where d is the dimensionality of the tensor.

5.1.2 Example persistence diagram

Consider a 2D tensor $T = \begin{bmatrix} 1 & 3 & 2 \\ 4 & 1 & 5 \\ 2 & 6 & 3 \end{bmatrix}$

1. Flatten and sort the values: $[1, 1, 2, 2, 3, 3, 4, 5, 6]$, keeping track of their locations.
2. Process the points.
 - (a) At $t = 1$: Two components are born (local minima at positions $(1, 1)$ and $(2, 2)$).
 - (b) At $t = 2$: The components at $(1, 3)$ and $(3, 1)$ merge with existing components.
 - (c) At $t = 3$: The components at $(1, 2)$ and $(3, 3)$ merge with existing components.
 - (d) At $t = 4$: The component at $(2, 1)$ merges with the component at $(1, 1)$.
 - (e) At $t = 5$: The component at $(2, 3)$ merges with the component at $(2, 2)$.
 - (f) At $t = 6$: The component at $(3, 2)$ merges with the component at $(2, 2)$.

The persistence diagram will have points $(1, 2), (1, 3), (1, 4), (1, 5), (1, 6)$.

5.1.3 Wasserstein distance

The Wasserstein distance (also known as the earth mover’s distance) between two persistence diagrams is a measure of the cost of transforming one diagram into the other.

The Wasserstein distance between two persistence diagrams D_1 and D_2 is defined as $\inf_{\gamma} (\sum_{(x,y) \in \gamma} \|x - y\|^p)^{\frac{1}{p}}$ where γ is a matching (bijection) between the points of D_1 and D_2 , $\|x - y\|$ is the Euclidean distance between points x and y , and p is the order of the Wasserstein distance (typically $p = 1$ or $p = 2$).

To compute the Wasserstein distance between two persistence diagrams D_1 and D_2 :

1. Add projections of all points in D_1 and D_2 onto the diagonal $b = d$ to ensure the two diagrams have the same number of points. Let D'_1 and D'_2 be the augmented diagrams.
2. Compute the pairwise Euclidean distances between all points in D'_1 and D'_2 . This results in a cost matrix C , where $C_{ij} = \|x_i - y_j\|$ for $x_i \in D'_1$ and $y_j \in D'_2$.
3. Find the optimal matching γ that minimizes the total cost $\sum_{(x,y) \in \gamma} \|x - y\|$.
4. Sum the costs of the optimal matching and take the p -th root.

Time and memory complexity

If n is the number of pairs, the time complexity of computing the Wasserstein distance is dominated by solving the assignment problem: The cost matrix construction can be parallelized to $O(n)$ with infinite threads. However, the Hungarian algorithm is inherently sequential, and no known parallel algorithm can reduce its complexity below $O(n^2)$. Thus, the overall time complexity is $O(n^2)$.

The cost matrix takes $O(n^2)$ space and the Hungarian algorithm requires $O(n^2)$ space.

Thus, the total memory complexity is $O(n^2)$.

5.2 Hyperparameters used

Table 4 shows hyperparameters used for all experiments. For details, see the code.

5.3 Choosing sharpness

Setting the sharpness hyperparameter s can be tricky. We provide the following suggestion as a starting point: Set s as a trainable parameter, and find the loss between random examples in the relevant dataset using an appropriate loss function, e.g. MSE loss for images. The MSE loss will tend toward some value. Then use stochastic gradient descent to minimize the difference between DSL and the reference loss function. Pseudocode is in Algorithm 2.

5.4 Shallow water reconstruction example

Figure 7 shows an example from the shallow water simulation dataset and its reconstructions using varying mixtures of MSE and DSL.

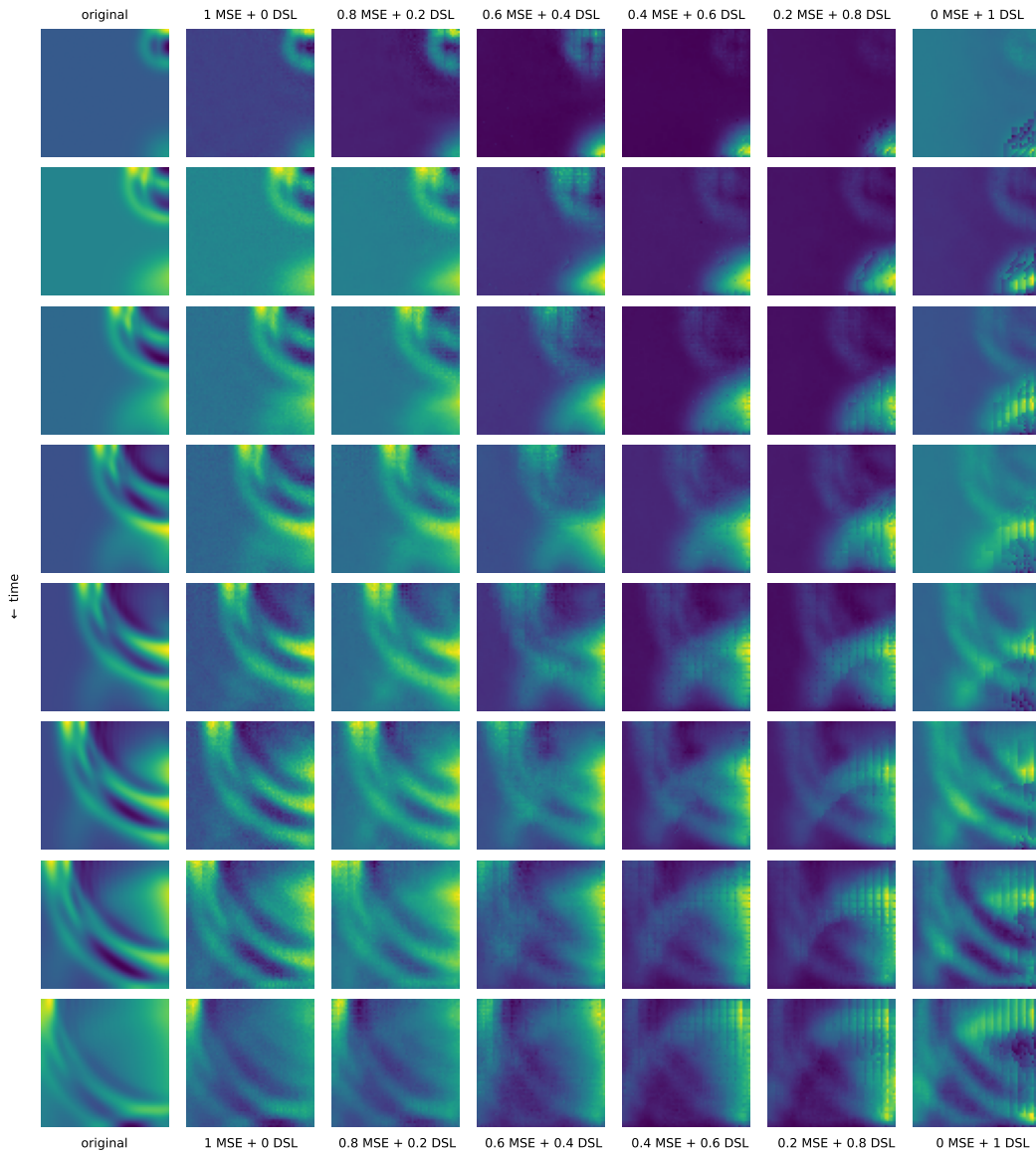


Figure 7: Original shallow water simulation snapshots and reconstructions. Column labels show DSL weights (which are $1 - \text{MSE weights}$) in the combined loss function used during training.

Table 4: Hyperparameters used for experiments. Layer or filter counts and sizes are given as *encoder*; *decoder*. †For the Duan et al. [2024] model, they are: Number of filters: 3, 7, 6, 1, 6, 1, 4; 1, 8, 3, 2, 3, 4, 8. Filter sizes: 4, 7, 7, 2, 7, 2, 5, 2, 3; 1, 3, 5, 3, 7, 3, 7, 3, 7. Strides: 4, 1, 1, 2, 1, 2, 1, 2, 2; 1, 1, 1, 2, 1, 1, 2, 1, 1. Adam is [Kingma and Ba, 2017], He initialization is [He et al., 2015], and GELU is [Hendrycks and Gimpel, 2023].

| Experiment | Demonstration § 3.3 | Stock prices § 4.1 | Images § 4.2 | Simulation § 4.3 |
|-----------------------------|---------------------|--------------------|---------------------------|-------------------------|
| Model architecture | MLP | MLP | Duan et al. [2024] | CNN |
| Number of layers or filters | 2; 2 | 2; 2 | † | 64, 128; 128, 64 |
| Layer or filter sizes | 32; 32 | 2048; 2048 | † | 3, 3; 3, 3 |
| Input size | 2048 | 64 | $3 \times 256 \times 256$ | $8 \times 64 \times 64$ |
| Latent dimension | 2 | 32 | 512 | 4096 |
| Activation function | ReLU | ReLU | GELU | ReLU |
| Optimizer | Adam | Adam | Adam | Adam |
| Scheduler | none | none | cosine annealing | 0.5 on 20 plateau |
| Initialization | He | He | He | He |
| Learning rate | 0.001 | 0.0001 | 0.0002 | 0.0001 |
| Dropout rate | 0 | 0 | 0 | 0.1 |
| Batches | 20000 | 64000 | 50000 | 10000 |
| Batch size | 1024 | 64 | 32 | 64 |
| Regularization | 0 | 0 | None | 0 |
| Sharpness | 32 | 16 | 9.6 | 16 |

Algorithm 2: Find Sharpness

Input: Dataset \mathcal{D} , reference loss L_{ref} , maximum steps T , stopping threshold ϵ

Output: Optimized sharpness parameter s

Initialize s as a trainable parameter;

Set optimizer \mathcal{O} ;

for step $t \leftarrow 1$ **to** T **do**

Randomly sample a batch $\mathcal{B} \subset \mathcal{D}$;

Split \mathcal{B} into random subsets \mathcal{B}_1 and \mathcal{B}_2 ;

Compute the reference loss;;

$$\ell_{\text{ref}} \leftarrow L_{\text{ref}}(\mathcal{B}_1, \mathcal{B}_2)$$

Compute the DSL loss using s ;;

$$\ell_{\text{DSL}} \leftarrow \text{DSL}(\mathcal{B}_1, \mathcal{B}_2, s)$$

Compute the optimization loss;;

$$\ell_{\text{opt}} \leftarrow (\ell_{\text{DSL}} - \ell_{\text{ref}})^2$$

Backpropagate ℓ_{opt} to compute gradients of s ;

Update s using \mathcal{O} and reset gradients;

if $\ell_{\text{opt}} < \epsilon$ **then**

| **break**;

return s
